



()

Performance Measurements of a Rotating Magnetic Field Thruster

Joshua M. Woods*, Christopher L. Sercel†, Tate M. Gill‡, and Benjamin A. Jorns§
University of Michigan, Ann Arbor, MI, 48109

The performance of a 1.1-kW rotating magnetic field (RMF) thruster is experimentally characterized. The performance, as indicated by the thrust and energy coupling efficiency, was parametrically investigated by varying the thruster flow rate, pulse frequency, and applied magnetic field strengths. The thruster was operated at steady state. Total power levels ranged from 32 W to 1.1 kW. The total and RMF-generated thrust were measured using a null type inverted pendulum thrust stand. Coupling efficiencies were calculated by measuring the discharge current waveforms for vacuum and plasma loaded cases and determining how much energy was deposited into the plasma. At a power level of 32 W, the maximum coupling efficiency was approximately $4.24 \pm 0.89\%$. No statistically significant thrust was measured. Potential reasons for this low performance are discussed in the context of strategies for increasing thruster performance. It is likely that poor seed plasma diffusion to the walls and lower discharge currents across the coils resulted in poor coupling efficiencies.

I. Nomenclature

B	=	magnetic field
C	=	capacitance
e	=	elementary charge
E_0	=	input energy
E_P	=	energy deposited into plasma
f	=	pulse frequency
F_z	=	axial force
j	=	plasma current
I	=	current
\dot{M}	=	mass flow rate
n	=	plasma density
R	=	resistance
T	=	thrust
V	=	voltage
δ	=	skin depth
η_c	=	coupling efficiency
ω	=	rotating magnetic field frequency
ω_{ce}	=	electron cyclotron frequency
ν_{ei}	=	electron-ion collision frequency

*PhD Candidate, Department Name, 1320 Beal Ave, Ann Arbor, MI 48109, AIAA Student Member

†PhD Candidate, Department Name, 1320 Beal Ave, Ann Arbor, MI 48109, AIAA Student Member

‡PhD Candidate, Department Name, 1320 Beal Ave, Ann Arbor, MI 48109, AIAA Student Member

§Assistant Professor, Aerospace Engineering, 1320 Beal Ave, Ann Arbor, MI 48109, AIAA Senior Member

II. Introduction

Electric propulsion (EP) thrusters have seen a steady increase in use over recent decades. EP devices offer an efficient method of propulsion due to their high specific impulses which, on average, can be more than an order of magnitude than chemical rockets [1]. Current satellites implementing EP typically use ion and Hall thrusters which offer reasonable efficiencies and thrust at powers on the order of 1 kW and below. Despite the heritage of these thrusters, there is a need for devices that can operate at the 100 kW - 1 MW range while retaining a relatively high thrust-to-mass ratio. Such power levels will enable large unmanned and manned payloads to be shuttled beyond cislunar space. A compelling class of thrusters that fit this profile are inductive pulsed plasma thrusters (IPPTs). While Hall thrusters currently have a power scaling of 0.5 kW/kg, IPPTs can theoretically reach upwards of 20 kW/kg [2]. In addition, IPPTs are propellant-agnostic which not only makes the thruster more flexible in its operation, it also allows it to be used in conjunction with in-situ resource utilization technologies. IPPTs also have the advantage of being able to vary the specific impulse and thrust independently—the specific impulse is a function of the operating conditions of each pulse while the thrust is proportional to the pulse rate [3]. This ability to vary power while maintaining efficiency is particularly attractive for rapid repositioning of assets.

The operation of all IPPTs are predicated on the ability to induce a current in the plasma that acts via a Lorentz force to accelerate the propellant. While there are multiple mechanisms for achieving this, one particularly promising candidate for high power electric propulsion is the rotating magnetic field (RMF). This concept is based on driving a current in an axisymmetric plasma by applying a rotating magnetic field that drags the electrons in a closed drift. In contrast to other types of inductive acceleration processes (e.g. theta-pinch configurations), the RMF current drive process does not rely on the generation of large transient voltages. This feature in principle overcomes a known lifetime limitation of pulsed thrusters where the high voltage requirements can lead to rapid degradation of components [4].

Given the potential advantages of IPPTs and RMF devices, there have been a number of previous efforts to develop and concepts based on this principle [5–8]. However, despite the significant fundamental insight into the RMF process that has emerged from these previous studies, practically there is still an open question as to how effective these devices are as thrusters. Indeed, while there have been attempts to measure performance of these devices indirectly with downstream sensors [6], to our knowledge there has been no published *direct* (i.e. on a thrust stand), steady-state thrust measurements of these devices to date. The lack of direct performance data represents a critical missing step in the development of this technology. Without quantitative and direct measures of performance, it is not clear what the current state of the technology is or how the efficacy of design improvements can be assessed. The need is apparent for robust test articles and facilities to parametrically evaluate RMF thruster performance.

To address this need, the goal of this work is to present direct performance measurements of a new RMF thruster in a high vacuum environment. With this end in mind, this paper is organized in the following way. The first section provides an overview of the theory of RMF theory of operation and scaling laws for performance. The second section describes the experimental setup, including the thruster, facility, and power delivery system. In the third section, we present results of operating the thruster at a variety of conditions. Finally, we analyze various trends identified in the collected data and use them to outline various techniques to increase RMF thruster performance.

III. Theory of Operation

As the operation and performance of RMF thrusters remains poorly understood, one of the key goals of our study is to explore parametrically how thruster behavior varies. This invites the question for the design of our test article and experimental setup as to which parameters we should attempt to vary to impact performance. The goal of this section is to motivate this based on the leading theory of operation of these devices.

To this end, we first overview the principle of operation of current drive through RMF thrusters. This model is based on the derivation first presented by Blevin and Thonemann [9]. The key elements in the formation process are illustrated in Fig. 1. Neutral gas with a small amount of seed plasma from a pre-ionizer fills the discharge chamber. This plasma is confined by a steady background magnetic field with a radial gradient, given in cylindrical coordinates as

$$\mathbf{B}_s = B_{s,r}\hat{\mathbf{r}} + B_{s,z}\hat{\mathbf{z}}, \quad (1)$$

where B_s denotes the steady background magnetic field and $B_{s,r}$ and $B_{s,z}$ are its radial and axial components respectively.

Two sets of saddle coils are oriented perpendicular to each other, and phase-shifted currents with frequency ω are driven through these coils, generating alternating magnetic fields that are 90° out of phase. The combined effect of

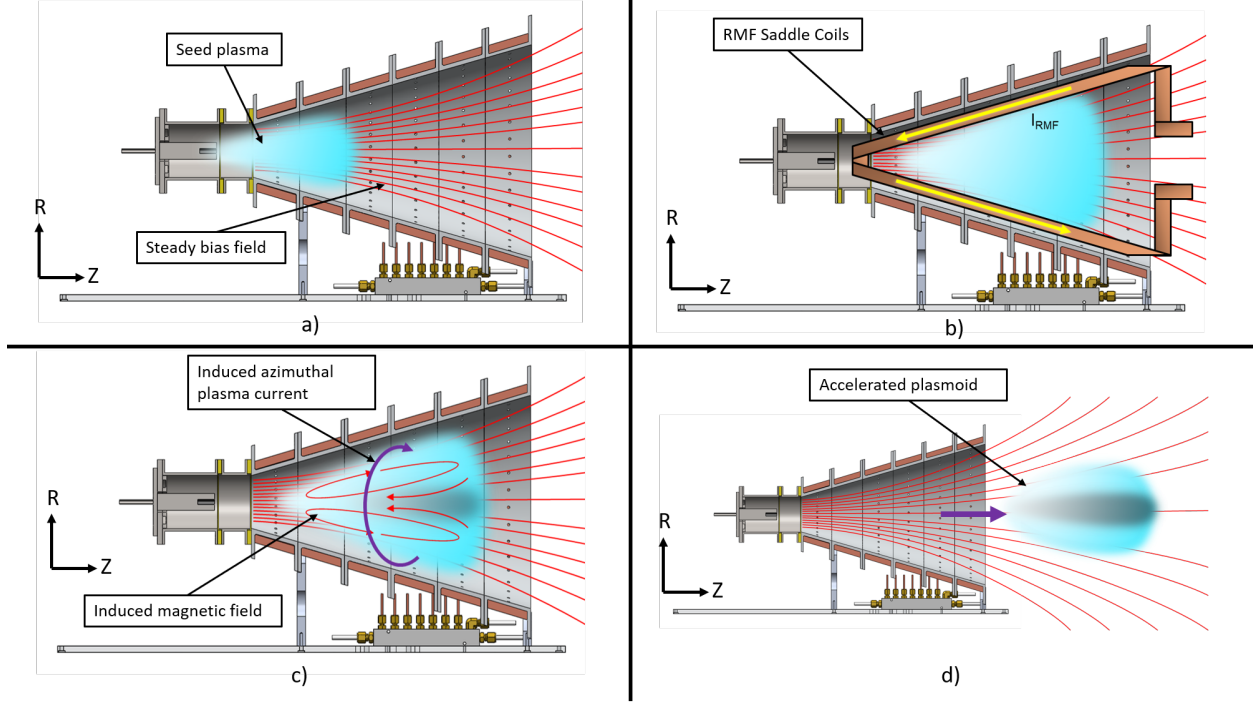


Fig. 1 RMF Operation: a) Side view cross-section in the r - z plane of the thruster illustrating how ionized gas is injected into the discharge chamber. A steady bias magnetic field with radial gradient is present. b) The RMF coils are discharged. c) An azimuthal current is generated in the plasma, which also induces an opposing magnetic field. d) The plasma is accelerated out of the thruster.

these coils creates a RMF of the form

$$\mathbf{B}_{RMF} = B_o \cos(\omega t) \hat{\mathbf{x}} + B_o \sin(\omega t) \hat{\mathbf{y}}, \quad (2)$$

where B_o is the amplitude of the magnetic field. While a real RMF would have spatial variation, this idealization of the field does not. The RMF frequency should be much greater than the ion cyclotron frequency but much less than the electron cyclotron frequency to ensure that the induced ion currents are much smaller than the electron currents. The combination of Faraday's law of induction and the generalized Ohm's law for an infinitely long plasma column show that the time varying RMF magnetic field produces an electric field that in turn drives an azimuthal plasma current. The electron Hall parameter is defined as $\Omega_e = B_o / (\eta n_e e)$, where η is the plasma resistivity, n_e is the electron density, and e is the elementary charge. In the limit of low plasma resistivity, Ω_e will be much greater than one, and the electrons will rotate in sync with the RMF. In this case, the plasma current density as a function of radial position is:

$$j_\theta(r) = -n_e e \omega r, \quad (3)$$

where n_e is assumed constant.

The above formulation, specifically Eq. (3), illustrates a key advantage of RMF thrusters. In principle, if the resistivity is sufficiently low, the current that is driven in the azimuthal direction is independent of the current in the driving coils.

There are three theories proposed for the thrust generation mechanism in an RMF thruster: Lorentz force produced by an applied field, self-field acceleration, and thermal-to-kinetic energy conversion. While it is unknown how much each contributes to overall thrust, simple scaling models can reveal operational parameters that can be tuned to increase performance. The Lorentz force is produced by the interaction of the azimuthal current driven by rotating magnetic field and the radial component of the steady background magnetic field. This equation can be expressed as

$$F_z = \int_V J_\theta B_{s,r} dV. \quad (4)$$

The integral is performed over the plasma volume. From Eq. (3), the azimuthal current scales with ω and n_e . The former variable is set by the power supply while the latter can be controlled experimentally by changing the flow rate. The maximum azimuthal plasma current density is achieved for a sufficiently strong RMF, which is proportional to the current through the coils [7]. Thus, the thrust due to Lorentz force as a function of tuneable parameters is

$$T_{AF} = F(\dot{m}, \omega, I_{RMF}, I_{B_s}, f), \quad (5)$$

where \dot{m} is the mass flow rate, I_{RMF} is the RMF coil current, and I_{B_s} is the steady background magnetic field coil current. We have also introduced the pulse rate, f , which is key for controlling thrust regardless of the acceleration mechanism.

The self-field acceleration component may also contribute to overall thrust. Theoretically, it is caused by a self-induced radial magnetic field. The resulting thrust would scale as $F_z \propto J^2$ where J is the plasma current (c.f. [10]). Based on Eq. 3, the self-field acceleration thrust is a function of the operational parameters: mass flow rate, RMF frequency, and RMF coil current:

$$T_{SF} = F(\dot{m}, \omega, I_{RMF}, f). \quad (6)$$

The RMF thruster may also convert its thermal energy to kinetic via adiabatic expansion through the magnetic nozzle. In this case, the flux conservers work to prevent thermal losses to the walls of the chamber and instead redirect this energy into directed thrust [11]. The kinetic energy of the propellant (and by extension the force) is related to the change in the enthalpy of the plasmoid as it is accelerated. The thrust would be a function of the mass flow rate and pulse energy, E_o :

$$T_{Th} = F(\dot{m}, E_o, f). \quad (7)$$

Thus, using the theoretical models of thrust for each of the acceleration mechanisms noted above, we have identified key operational parameters that can be tuned to change performance.

$$T_{tot} = T_{AF} + T_{SF} + T_{Th} = F(\dot{m}, \omega, I_{RMF}, I_{B_s}, E_o, f). \quad (8)$$

In addition, the topology of the background field can be changed to alter coupling and acceleration physics. The variables identified in Eq. 8 serve as the primary parameters we would like to be able to tune in the test article in the following section.

IV. Experimental Setup

A. Thruster Overview

The operational parameters derived in Section III require a highly configurable test article to perform studies over the parameter space identified in Eq. 8. To this end, the UM RMF thruster was designed to operate over a wide range of conditions. Fig. 2 shows an image of the thruster. It consists of three subsystems: the pre-ionizer assembly, bias field coils, and RMF coils. We discuss each in detail in the following sections.

Pre-ionizer assembly:

We selected a Lanthinum Hexaboride (LaB6) hollow cathode (Fig. 3a) for the pre-ionizing source of the RMF thruster. This cathode, which was designed for a Hall thruster, nominally operates at 20 A at 15 sccm [12]. Surrounding the opening of the cathode is a series of 40 orifices in a ring pattern that function as neutral injectors. The injectors are intended to provide up to 400 sccm of flow. Fig. 3b shows a zoomed-in view of the assembly.

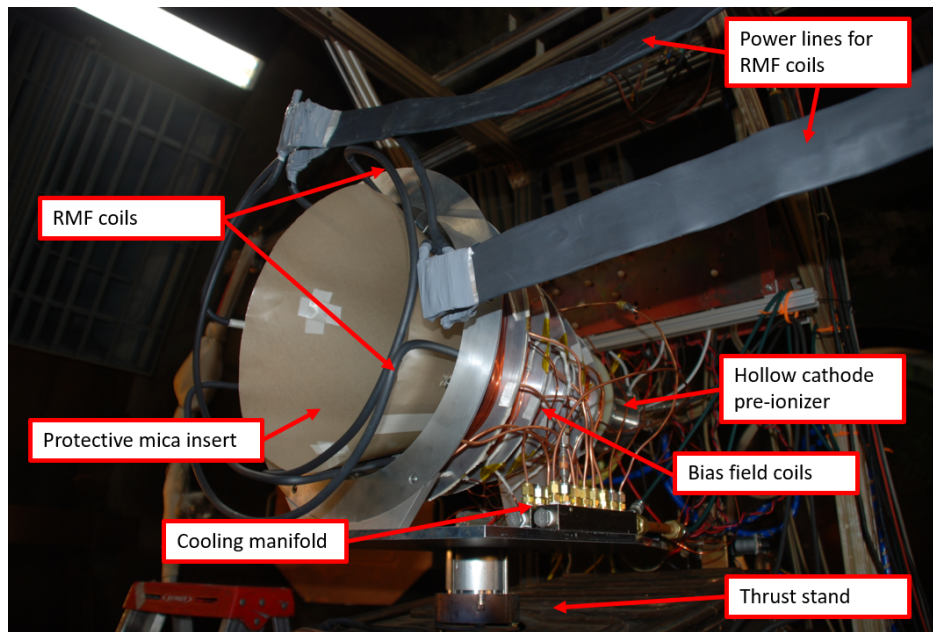


Fig. 2 RMF thruster installed on an inverted pendulum thrust stand in the Large Vacuum Test Facility at the University of Michigan.

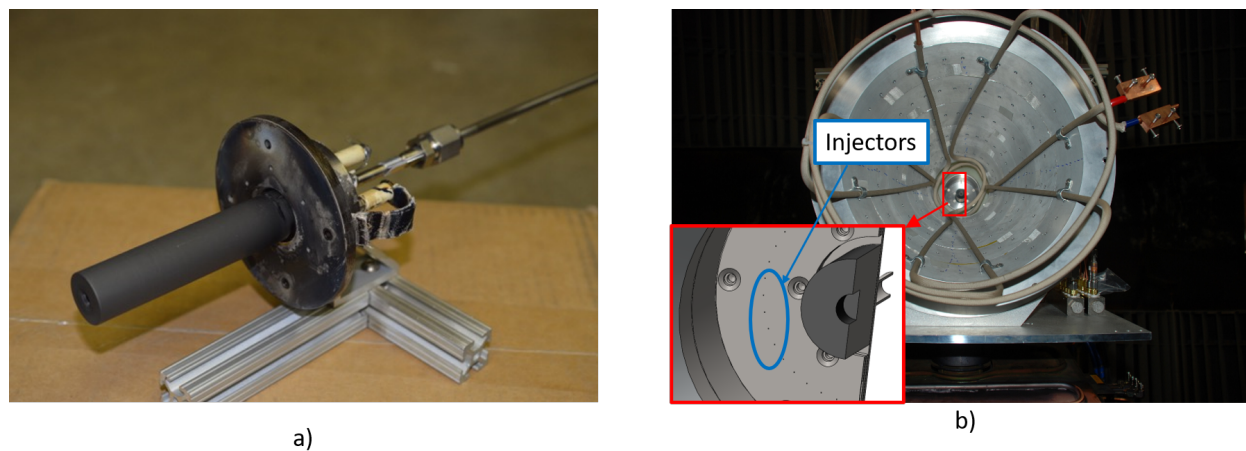
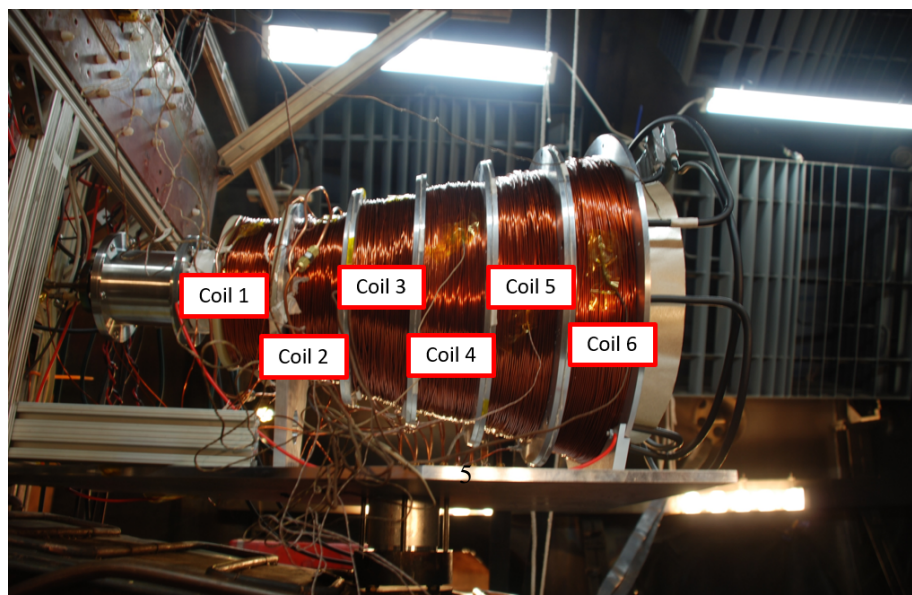


Fig. 3 a) LabB6 hollow cathode employed as a pre-ionizer for the UM RMF thruster. b) Zoomed in view of cathode assembly installed in thruster showing neutral injectors (circled in blue).



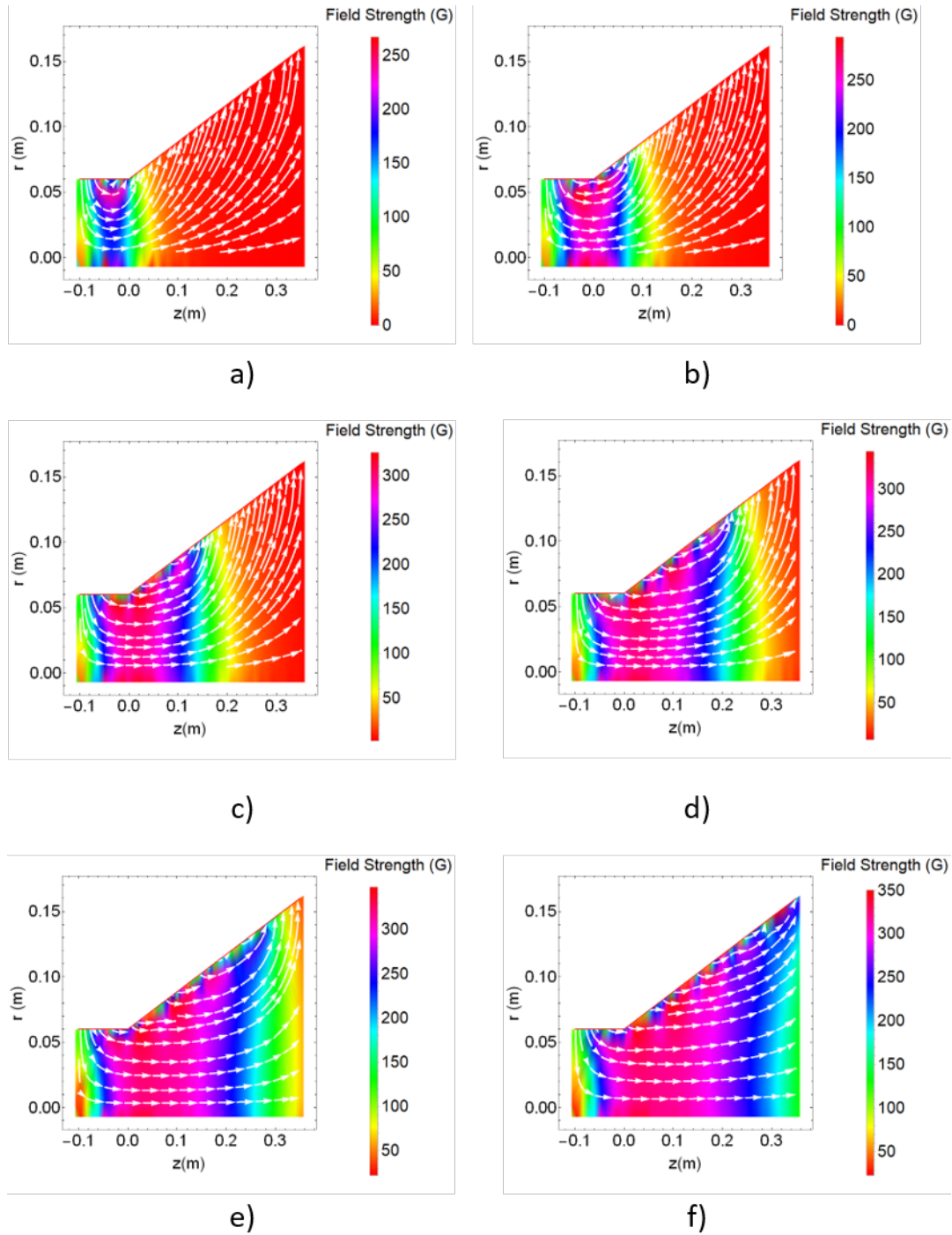


Fig. 5 Iso-polarity magnetic field configurations (all at 2000 A-turns). a) Coil 1 active b) Coils 1 and 2 active c) Coils 1, 2, and 3 active d) Coils 1, 2, 3, and 4 active e) Coils 1, 2, 3, 4, and 5 active f) All coils active (nominal configuration).

Bias field: The bias field is generated by six magnetic coils arranged conically that also make up the bulk of the thruster's physical structure as shown in Fig. 4a. The cone angle is 16° to provide the desired magnetic nozzle topology as shown in Fig. 4b. The first upstream coil is constructed using G10 to reduce coupling of the RMF coils. The other coils are made of aluminum bobbins which act as flux conservers. In theory, azimuthal currents in the plasma will induce mirror currents in the bobbins. This interaction will result in a magnetic force pushing the plasma radially inward,

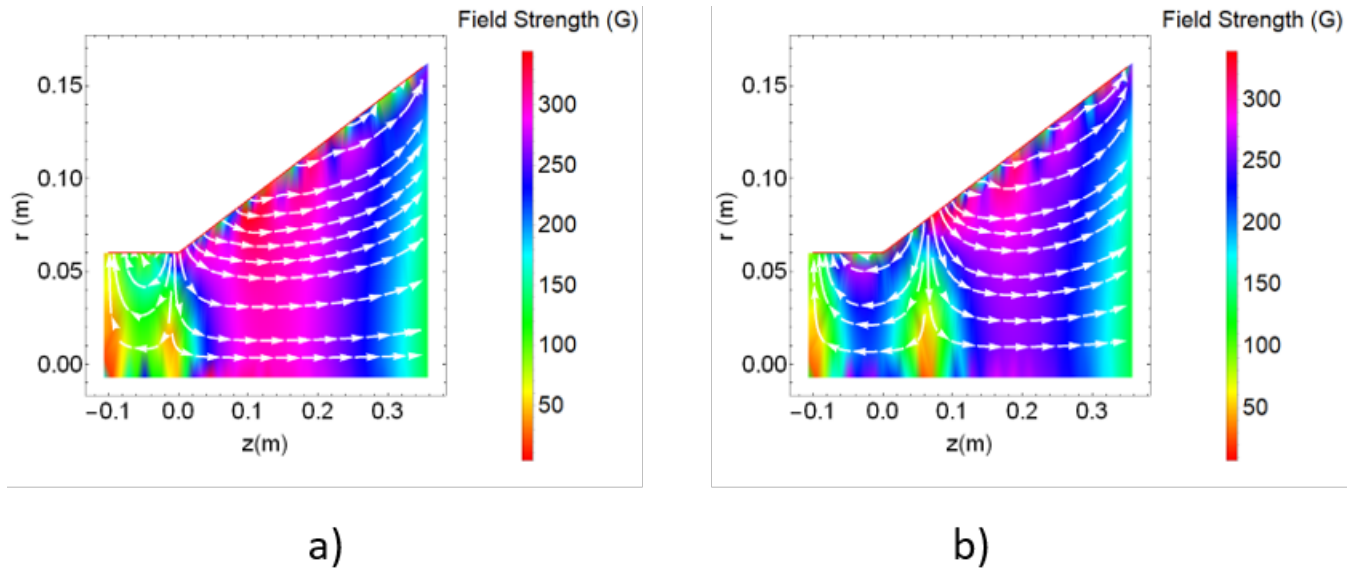


Fig. 6 Reversed polarity magnetic field configurations (all at 2000 A-turns). $z = 0$ is the intersection of coils 1 and 2. a) Coil 1 reversed polarity b) Coils 1 and 2 reversed polarity

thus keeping it off of the walls, as well as causing self-field acceleration axially. Each winding is designed to achieve 2000 A-turns at the 100% magnetic field setting, which corresponds to approximately 325 G on centerline. Cooling is embedded in each of the coils to prevent overheating of the magnet wires. In the nominal condition, all magnets have the same polarity. However, during our tests, the configurations of the magnets were sometimes be changed in an effort to better diffuse the seed plasma to the walls where the RMF coils are located. In theory, this would increase the coupling efficiency. The specific configurations are discussed in detail in Section V.

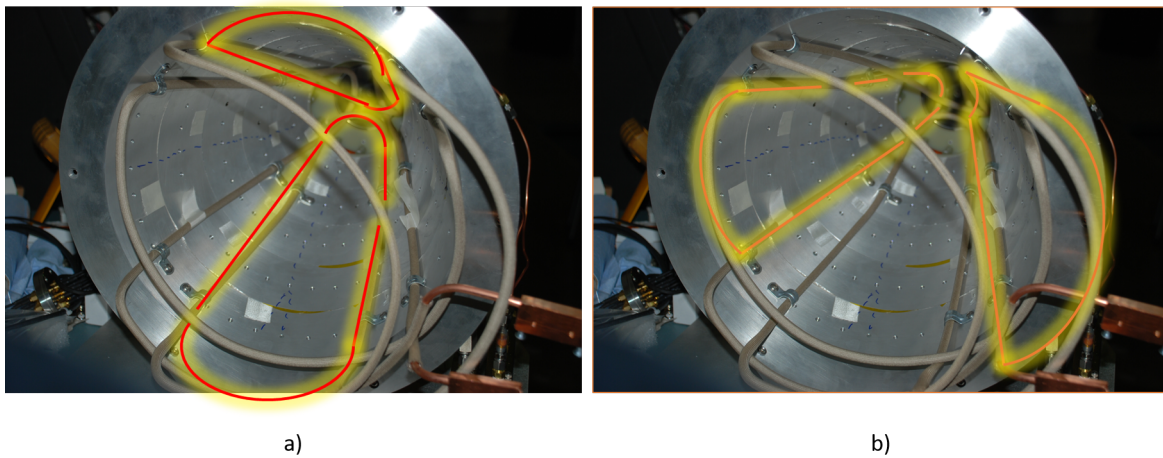


Fig. 7 The two sets of RMF coils fit nest inside the cone of the thruster.

RMF coils: The two RMF coils are comprised of copper tubing. The tubing allows the coils to be cooled during high powered operation. The coils are bent to create two loops and are oriented orthogonal to each other as shown in Fig. 7. The coils conform to the sides of the thruster cone. The thickness of the tubing is much greater than the estimated skin depths expected during 20 kHz and 125 kHz RMF frequency operation. Appendix A provides RMF field maps at various axial positions to illustrate how discharging the coils can produce mostly uniform magnetic fields.

B. Power transmission lines

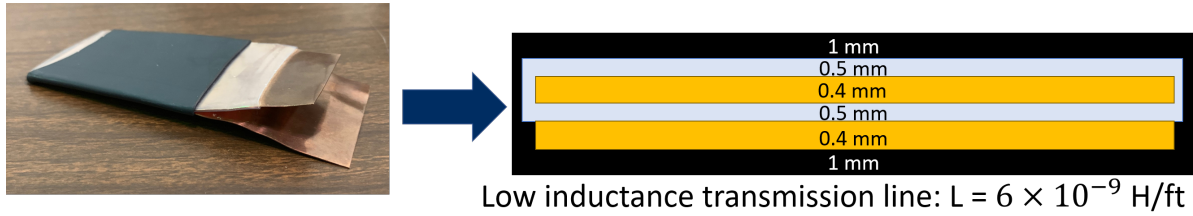


Fig. 8 Left: A photo of a section of low-inductance transmission line. Right: An illustration depicting of the cross section of the same.

To couple power into the coils, we designed and built custom low-inductance transmission lines. We require that the total inductance of the transmission line between the power processing unit and the antenna be less than 10% of the inductance of the coil. This ensures that a majority of the voltage drop occurs across the coils, and a lower inductance yields higher currents for a fixed voltage. Because each coil has an inductance of approximately $2.5 \mu\text{H}$, this limits the transmission line to 250 nH for its entire 22 ft length, or about 11 nH/ft. By holding pieces of copper sheet as close together as possible using heat shrink, we achieve 9 nH/ft using a broadside-coupled trace calculation. This puts the whole line at 130 nH for the entire length, or 5% of the coils. The use of these lines allows the power processing unit (PPU) to be placed outside of the chamber which eliminates issues pertaining to operating in vacuum.

C. Power Processing Units

To provide power to the RMF coils, we designed a custom PPU which consists of five distinct subsystems: a 150 kW high voltage supply, a low-pass filter, two identical LRC tank circuits, and a fiber-optic switching controller. Figure 9 shows the primary circuit diagram of the PPU.

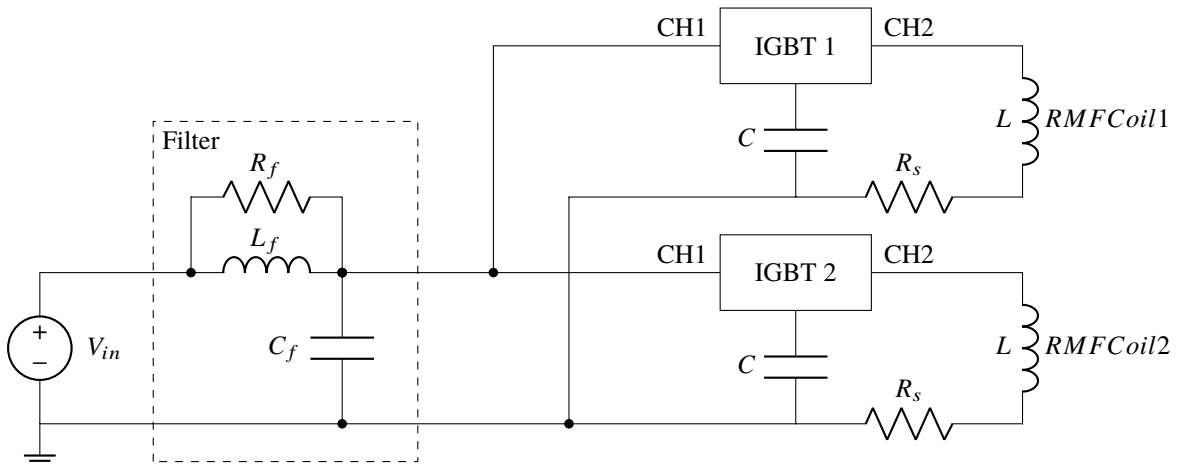


Fig. 9 PPU Schematic

The PPU operates by charging a capacitor bank for each coil to a commanded voltage before allowing it to ring down producing a waveform of a set frequency and damping factor. Two capacitor banks are used with capacitances of $24 \mu\text{F}$ and 660 nF to produce RMF frequencies of 20 kHz and 125 kHz respectively. We selected the Magna MT series 150 kW (1000 V, 150 A) supply for use in this system because of its high tolerance to ripple currents on its output capacitors, and the low-pass filter was implemented to further protect the DC supply from the large current transients from the pulsed power output. Each of the main LRC tank circuits is comprised of a dual channel insulated-gate bipolar transistor (IGBT) switch, L , in addition to the RMF coil, main capacitor bank, C , and stray resistance, R_s , in Fig. 9. The two IGBT channels permit independent charging and discharging of the main capacitor banks and are triggered

optically by a separate custom driver circuit. This driver circuit works in tandem with a commercial signal generator to command the IGBTs to discharge the capacitor banks at the desired pulse repetition rate and RMF phase offset. All high-voltage components are optically isolated from the control circuitry for safety, and water cooling is provided to the filter resistor and IGBT units due to the power losses seen by these components.

D. Thrust Stand

All thrust measurements were taken using a null-type inverted pendulum thruster with water cooling to reduce thermal drift as shown in Fig. 2. The thrust stand was calibrated using a set of known weights and is also inclination-controlled. It has been used to test other high power electric propulsion devices such as the H9, 9 kW class Hall thruster, and the N30, a 30 kW class Hall effect thruster [12]. Despite the RMF thruster being a pulsed device, pulse rates > 100 Hz produce quasi-steady thrust and are well above the stand's resonance frequency, enabling us to use thrust stands nominally used for steady state thrusters [13].

Each thrust measurement begins by recording the null coil current at a specific thruster operating condition (e.g. cathode on only) and the inclination control active for 30 seconds. Then, the inclination control is turned off. This reduces the noise associated with the inclinometer stepper motors. The null coil current is recorded for a further 30 seconds before the thruster operating condition is changed, (e.g. turning the RMF on) resulting in a change in recorded current which corresponds to the thrust output. Null current is recorded for another 30 seconds with no inclination control before the inclinometer is activated again for another 30 seconds. The Δ -current is calculated by averaging the null coil currents immediately before and after the change in thruster operation and subtracting the two averages from each other. The variance in the averages is the uncertainty. An inclination correction must be performed to account for phantom current induced by slight changes in the inclination during the thrust measurements. This is accomplished by creating a calibration curve relating the current measured by the coils at different inclinations and using it to subtract out the corresponding current caused by the average inclination of a thrust measurement.

E. Large Vacuum Test Facility



Fig. 10 UM Large Vacuum Test Facility

Tests were performed in the University of Michigan's Large Vacuum Test Facility (LVTF). LVTF is a 6 m diameter by 9 m long chamber (Fig. 10). It is capable of reaching a base pressure of 10^{-8} torr through the use of 19 cryopumps. The pumping speed with all pumps running is approximately 500,000 L/s on xenon including conductance losses. Pressure is measured with a xenon calibrated Stabil ion gauge mounted 1 m away from the thruster exit plane [14].

V. Results

The UM RMF thruster was operated over a wide range of conditions ranging from powers of 32 W to 1.1 kW, flow rates of 25 sccm to 200 sccm, magnetic fields from $x\%$ to 100% of the nominal operating condition, various phase angles between the RMF discharges, and numerous magnetic field topologies. Table 1 provides an overview of the

parameter space explored during the experimental campaign. In the following subsections, we present the thrust and coupling efficiency results. All tests were performed using xenon gas.

Parameter	Conditions
Total Flow Rate	25, 50, 100, and 200 sccm (15 sccm through cathode, rest through neutral injectors)
RMF Frequency	20 and 125 kHz
Bias Magnetic Field Strength	33%, 66%, and 100% (also reversed polarity in some cases)
Power levels	32 W to 8.1 kW
Bias Magnetic Field Topology	Cusp and solenoidal
Phase Angle	-90° to 90°

Table 1 Notional Parameter Space

The thrust values for the initial flow studies at 1.1 kW represent the total (cathode plus RMF) thrust generated by the thruster. That is, the thruster was on with cathode and injector flow with the RMF active before being switched off by turning off the flow and power. The resulting change in measured null coil current corresponds to the total thrust produced. For all others, thrust generated only by the activation of the RMF was calculated to better resolve its contribution to performance. In this case, two thrust measurements were taken for each condition. The first occurs when the RMF is switched on while the second happens when the RMF is turned off. The two measurements are then averaged.

The coupling efficiency, η_c , is defined as the energy deposited in the plasma, E_P , divided by the initial energy stored in the capacitor banks, E_0 . The power is dissipated over either the plasma, the PPU resistance, or both. Assuming constant resistances, the energy conservation for the vacuum and plasma loaded shots respectively are:

$$E_0 = R_{PPU} \int_0^\infty I_V^2 dt, \quad (9)$$

$$E_0 = (R_{PPU} + R_P) \int_0^\infty I_P^2 dt. \quad (10)$$

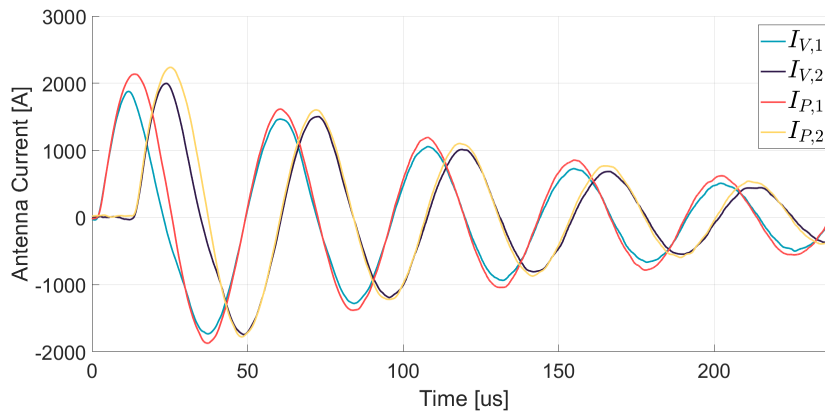


Fig. 11 Sample ringdown of the capacitor banks for vacuum and plasma loaded shots. Operating conditions: 750 V, 20 kHz RMF, 600 Hz pulse rate, 100 sccm, 100% B-field

I_V and I_P are the current traces measured by an oscilloscope during operation as shown in Fig. 11. E_0 is simply the energy initially stored in both capacitor banks and is equal to $\frac{1}{2}CV_0^2$. Therefore, using Eqs. 9 and 11 and recognizing that E_P is $R_P \int_0^\infty I_P^2 dt$, η_c is then:

$$\eta_c = \frac{E_P}{E_0} = 1 - \frac{R_{PPU}(T_P) \int_0^\infty I_P^2 dt}{R_{PPU}(T_V) \int_0^\infty I_V^2 dt}, \quad (11)$$

where we have introduced temperature corrections for the PPU resistances. We measured temperature using thermal couples placed on the RMF coils. The uncertainty is calculated by accounting for the error inherent in the oscilloscope, the integration process using MATLAB, and the uncertainty in the temperature for the resistance corrections.

A. Initial Flow Studies at 1.1 kW

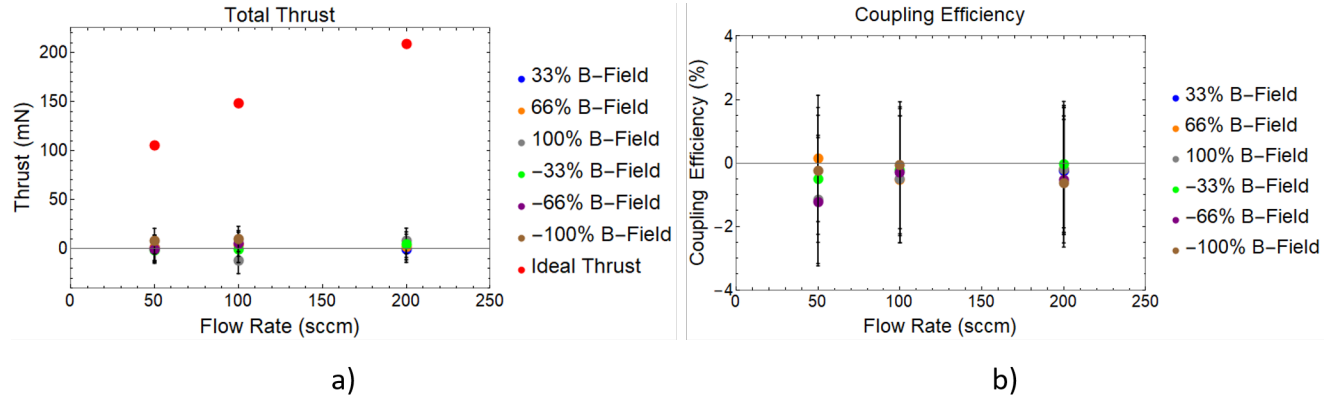


Fig. 12 Thrust and efficiency results at 1.1 kW (400 V, 20 kHz RMF, 300 Hz) at various flow rates and magnetic field settings. Constant operating conditions: a) Total thrust (ideal thrust assuming 100% efficiency in red) b) Coupling efficiency

Initial tests were performed using the 20 kHz capacitor bank charged to 400V and pulsed at 300 Hz. The flow and magnetic fields were varied to produce the thrust and coupling efficiency plots shown in Fig. 12. Ideal thrust assuming 100% efficiency is also plotted for reference. For all cases, thrust was negligible and the coupling efficiency was 0% when accounting for error bars.

B. Magnetic Field Topology Study

Configuration	RMF Thrust (mN)	Coupling Efficiency (%)
Nominal	8.53 ± 11.28	2.27 ± 0.90
Coil 1 Reversed Polarity	0.59 ± 11.36	0.42 ± 0.92
Coils 1 and 2 Reversed Polarity	-8.52 ± 0.58	0.92 ± 0.92

Table 2 Magnetic field topology study results.

In an attempt to increase performance beyond what was measured during our tests at 1.1 kW, we conducted a study to investigate how changing the magnetic field structure would affect performance. The magnetic field was changed by reversing the polarity of the first and second magnetic field coils (where the first is the most upstream coil). In theory, this would help quickly diffuse the seed plasma towards the RMF coils where they would aid in the ionization process, thus coupling more energy into the plasma. The three coil settings are: 1) nominal case in which all magnets have the same polarity (Fig. 5f), 2) coil 1 operated with reversed polarity (Fig. 6a), and 3) coils 1 and 2 operated with reversed polarity (Fig. 6b). Thrust and efficiency results are provided in Table 2. The operating conditions were 125 kHz RMF frequency, 65 W, 100 sccm, 100% B-field strength, and 600 Hz pulse rate. Although thrust remained negligible, the nominal configuration measured a higher coupling efficiency than the other configurations by a factor of five.

C. Flow Studies with 125 kHz RMF Frequency

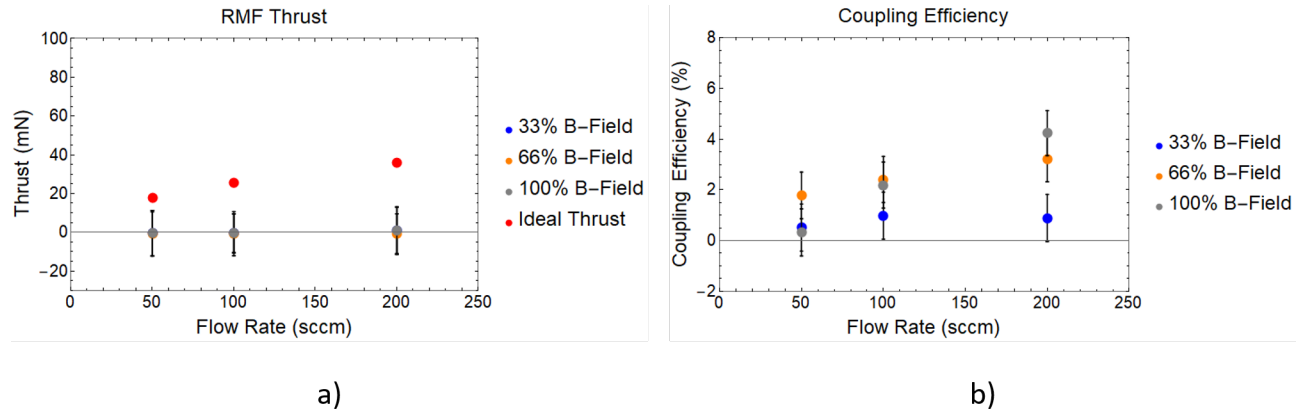


Fig. 13 Thrust and efficiency results at 32 W (400 V, 300 Hz pulse rate) at various flow rates and magnetic field settings a) Total thrust (ideal thrust assuming 100% efficiency in red) b) Coupling efficiency

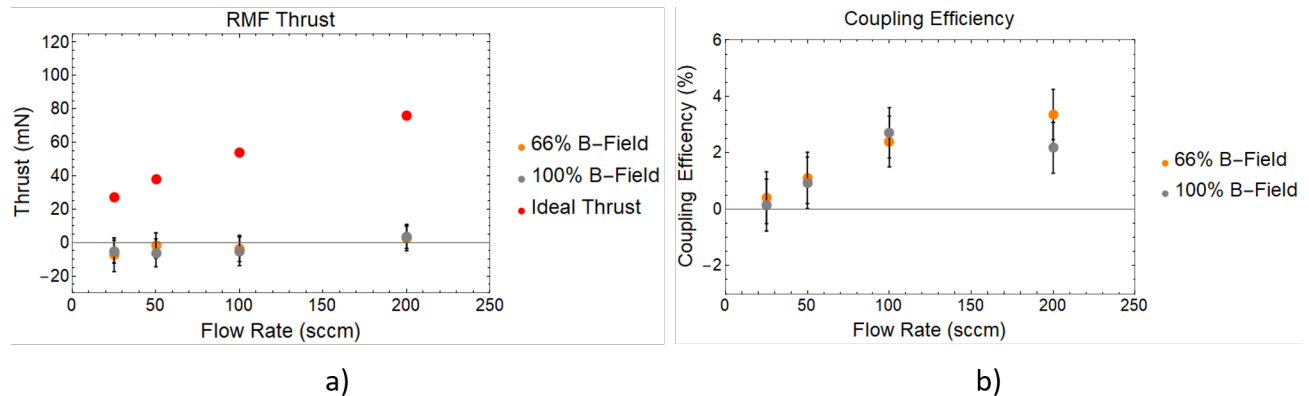


Fig. 14 Thrust and efficiency results at 146 W (600 V, 600 Hz pulse rate) at various flow rates and magnetic field settings a) Total thrust (ideal thrust assuming 100% efficiency in red) b) Coupling efficiency

Using results of the magnetic field topology study, we determined that the best magnetic field condition is the baseline configuration. With these conditions, flow and magnetic field variation tests were completed at power levels of 32 W, 146 W, and 228 W at 125 kHz RMF frequency. The pulse rate was 300 Hz for the 32 W operation and 600 Hz for all others. The power was also increased by increasing the voltage the capacitors were charged to (400 V, 600 V, and 750 V). Results are shown in Figs. 13 - 15. Although there is no appreciable thrust, we did observe trends in coupling efficiencies that we will discuss in the the following section.

D. Acceleration Region Studies

The magnetic field topology was shifted to change where the maximum radial magnetic field is located physically. This was accomplished by successively activating the bias coils to shift the expansion region of the magnetic nozzle in an effort to further increase diffusion of the seed plasma to the RMF coils. The individual magnetic field maps for each of the six configurations is provided in Fig 5. Other operating conditions were 125 kHz RMF frequency, 228 W, 100 SCCM, 100% B-field, and 600 Hz pulse rate. The results of the study are provided in Fig. 16. The coupling efficiency had large variations across the configurations with a peak when the first three coils were active which produced a magnetic field with a maximum radial component at $z = 0.14$ m. There was no measured thrust.

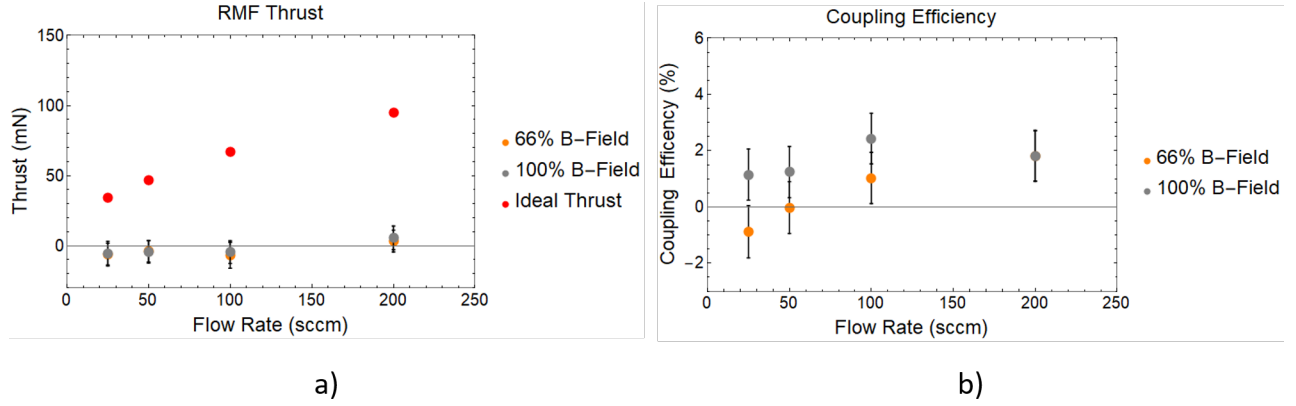


Fig. 15 Thrust and efficiency results at 228 W (750 V, 600 Hz pulse rate) at various flow rates and magnetic field settings a) Total thrust (ideal thrust assuming 100% efficiency in red) b) Coupling efficiency

E. 675 W Performance Measurements

We used the 20 kHz capacitor bank at a 50 Hz pulse rate and 750 V to achieve 675 W. This corresponds to 13.5 J per shot, the highest input energies of the test campaign. The acceleration region was changed by running the thruster with first the first three coils on (Fig. 5c) followed by the first two coils on (Fig. 5b) at 100 sccm, and the nominal magnetic field topology at 100% strength. The coupling efficiency and thrust were negligible (Fig. 17). We attempted to further push the thruster to 8 kW by increasing the pulse rate from 50 Hz to 600 Hz. However, this resulted in the power lines for the filter box melting before meaningful measurements could be taken. Trends observed in the experimental results will be discussed in the following section.

VI. Discussion

A. Reasons for Low Performance

For all conditions, coupling efficiency was low (below 5%) and thrust was negligible. There are likely two primary reasons for the low performance. The first is low peak currents. The highest current achieved during testing was approximately 2.3 kA. Weber found that for a device of similar size to the UM RMF thruster and operated with similar gas flows, a peak of nearly 10 kA was sufficient enough to achieve coupling efficiencies of 90% [6]. To gain further insight into whether the currents achieved in our experiment are sufficient to drive an azimuthal current in the plasma, we can use dimensionless criteria derived by Hugrass et al. [15]. They determined that for a steady state RMF acting on a semi-infinite plasma column of fixed density and shape, the field will penetrate into the plasma provided that

$$\left(\frac{\nu_{ei}}{\omega_{ce}}\right)^2 \left(\frac{R}{\delta}\right)^2 \ll 1, \quad (12)$$

where ν_{ei} is the electron-ion collision frequency, ω_{ce} is the electron cyclotron frequency, R is the radius of the plasma column, and δ is the skin depth. Essentially, Eq. 12 quantifies how strong the RMF should be in order to effectively penetrate the plasma. Although the expression is for a steady-state system, we can apply the criteria to our system to establish a benchmark for our RMF penetration values as shown in Fig. 19.

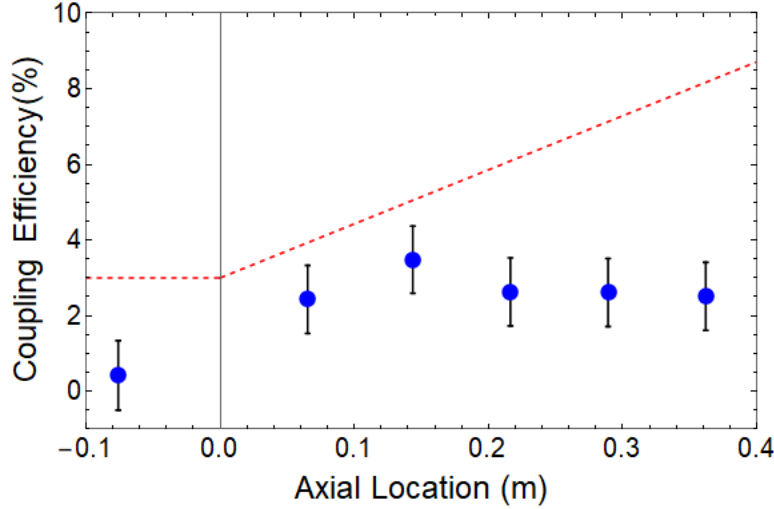


Fig. 16 Coupling efficiencies for magnetic field configurations representing different acceleration regions. The axial location corresponds to the position of maximum radial magnetic field for each magnetic field topology. The dashed red line is a notional indication of the thruster wall. Operating conditions: 125 kHz RMF frequency, 600 Hz pulse rate, 750 V, 100 sccm, 100% background magnetic field strength.

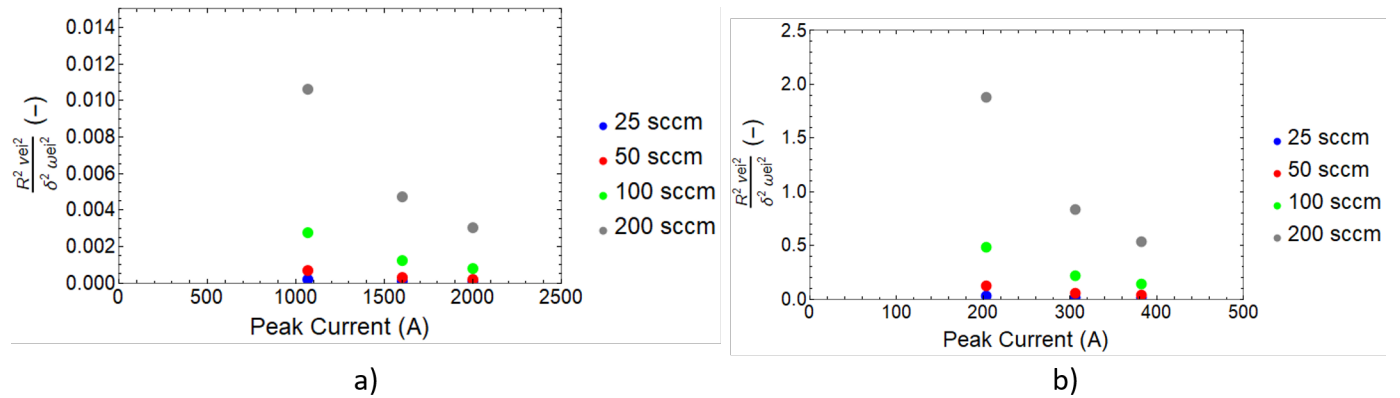


Fig. 19 Hugrass criteria for all operating conditions. a) 20 kHz capacitor bank b) 125 kHz capacitor bank

The density is calculated using the mass flow values. The RMF magnitude was calculated by measuring the field using a three-axis B-field probe. Measurements were taken within a 60 mm radius about centerline at the intersection of coils 3 and 4. The map is shown in Fig. 18. The value used to calculate ω_{ce} is the average of the measured points. The 20 kHz bank is consistently a 2 - 3 orders of magnitude below one, indicating that at the specified current levels, we should expect penetration of the RMF field into the plasma. However, it should be noted that this is peak current and is only achieved for an instant during discharge. Thus, the Hugrass criteria likely rapidly approaches one during discharge thus significantly reducing penetration. Similarly, the current levels of the 125 kHz bank consistently result in a Hugrass criteria of near or above 1 indicating poor penetration. Both cases point to poor coupling performance.

The second reason for poor coupling can be attributed to insufficient diffusion of the seed plasma and gas to the walls of the thruster where the RMF coils are located. For the nominal magnetic field configuration shown in Fig. 5f, the field lines do not diverge significantly from centerline until the thruster exit plane. As the cathode is located on centerline, the majority of the seed plasma will not readily diffuse to the walls. The electric field generated by the time varying currents in the coils decreases with the square of the distance from the coils. Thus, most ionization will occur close to the walls where the electric field is strongest. As was shown in the coupling studies, changing the topology of the magnetic fields has noticeable effects on the coupling efficiency as discussed below.

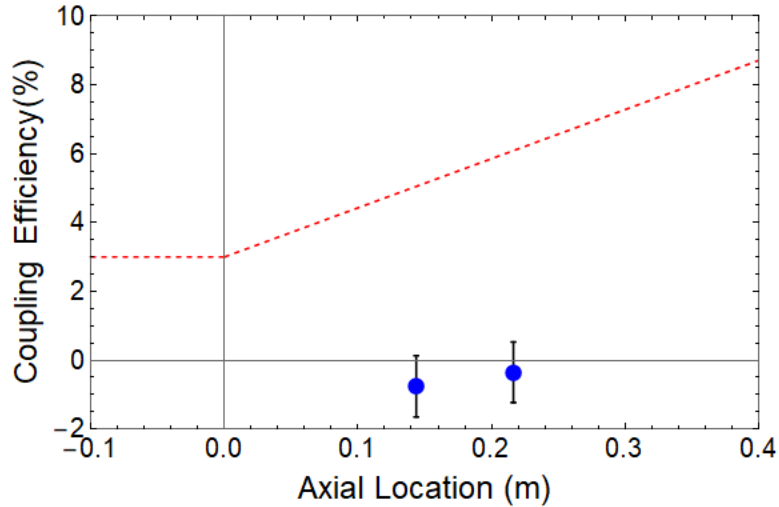


Fig. 17 Coupling efficiency results at 675 W. The axial location corresponds to the position of maximum radial magnetic field for different magnetic field topologies. The dashed red line is a notional indication of the thruster wall. Operating conditions: 20 kHz RMF frequency, 50 Hz pulse rate, 750 V, 100 sccm, 100% background magnetic field strength

B. Observed trends

Despite the low performance, several trends were observed over the course of testing that indicate possible optimal conditions for RMF thruster operation as shown by the flow and magnetic field strength studies in Figs. 12 - 15. For a fixed penetration depth of the RMF into the gas, a large flow rate results in a higher electron density that can be coupled to by the coils. Thus, total energy deposited into the plasma increases. A stronger background magnetic field could possibly be aiding in the diffusion of electrons towards the walls. For similar reasons, changing the magnetic field topology also increases the coupling efficiency in some cases. In particular, the acceleration region study showed that shifting the expansion region of the background field (Fig. 5) improves performance by nearly 50% compared to the nominal condition per Fig. 16. It is probable that more electrons are being diffused close to the walls, thus aiding in the ionization and acceleration process.

C. Limitations on power

Originally, the thruster was envisioned to operate at 1.5 kV. For the 20 kHz capacitor bank, this corresponds to 4 kA discharge currents across the RMF coils while for the 125 kHz bank, it would yield 750 A. The higher currents would produce stronger RMFs which would in turn help with penetration of the fields into the plasma thus increasing overall performance. The PPU was descoped due to issues with the snubber circuit which acts to protect the IGBTs from high voltage transients caused by the rapidly changing discharge currents. Thus, it was expected that performance would be poor given the low currents driven by the PPU.

D. Strategies for Improved Performance

Analyzing the coupling efficiency trends allows us to synthesize a few preliminary "rules of thumb" for RMF thruster operation. First and foremost, as indicated by the comparison of this experiment's results to that of Weber's [6], it is likely that running at the higher 4 kA discharge current will better drive and sustain a strong enough RMF to induce azimuthal currents in the plasma. Next, increasing flow and background magnetic field strength yields higher coupling efficiencies. Finally, some sort of plasma and/or gas diffusion apparatus is critical to increase coupling efficiency. This can be accomplished by tuning the magnetic field topology or by some other physical plasma diffusion device. Providing a path for electrons to travel close to the coils appears to increase performance.

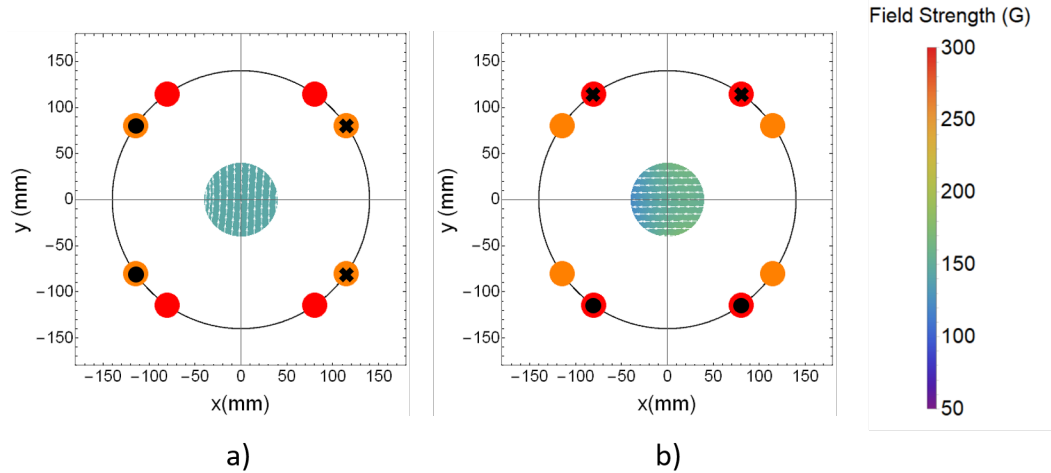


Fig. 18 Sample RMF B-field map for each coil. The B-field map within a 60 mm radius of the centerline was measured at the intersection of bias coils 3 and 4. Each plot represents one coil (consisting of two loops each) discharging at 2 kA. a) RMF coil 1 b) RMF coil 2

VII. Conclusions

We have presented performance measurements for the UM RMF thruster over a wide range of conditions at power levels up to 1.1 kW. Lack of performance data was highlighted as a key issue facing the EP community. RMF operation theory was reviewed to identify key parameters that can be tuned to change performance. These parameters guided the design that formed the basis of our experiment. The thruster was operated at a variety of conditions. Coupling efficiencies of less than 5% were observed for all cases and thrust was consistently negligible. However, increasing the background field strength and mass flow tended to increase the coupling efficiency. The low performance is likely due to a multitude of factors. Primarily, the driven current was insufficient to produce an RMF strong enough to penetrate the plasma and the seed plasma produced by the cathode did not sufficiently diffuse towards the walls. The physical insight gained by the trend analysis provides the basis for improving performance for future test articles.

VIII. Acknowledgements

We would like to acknowledge the technical support of Eric Vigas in the construction of the RMF thruster. We also would like to thank Dr. James Prager and Dr. Ken Miller from Eagle Harbor Technologies as well as Dr. Michael Homes of the Air Force Research Laboratory-Edwards and Prof. Justin Little for fruitful discussions about RMF thruster operation. This work was supported under an Air Fore SBIR program as well as an AFOSR Young Investigator Program award.

IX. Appendix

RMF Phase Study

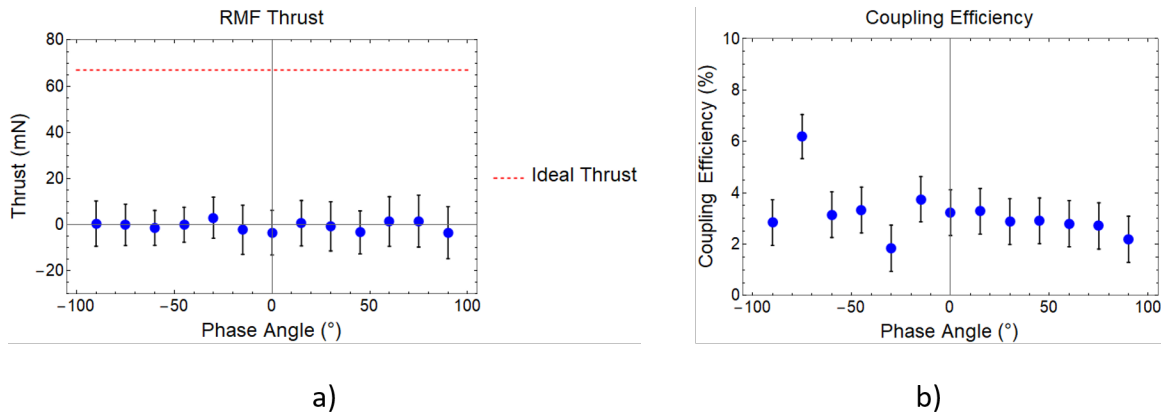


Fig. 20 Results for phase angle study (125 kHz RMF frequency, 65 W, 100 sccm, 100% B-field, and 600 Hz pulse rate.) a) RMF thrust (ideal thrust shown in red) b) Coupling efficiency

We performed a phase study to determine a more optimal condition for discharging the RMF coils. The phase angle relates the relative discharge timing between each of the coils. Initial testing showed that the two coils were coupling to each other and the magnitude of the coupling changed with the phase angle. The phase angle was varied from -90° to 90° in 15° increments. Operating conditions were 125 kHz RMF frequency, 65 W, 100 sccm, 100% B-field, and 600 Hz pulse rate. The bias field remained in its nominal configuration. Thrust and efficiency results are provided in Fig. 20. There is a broad peak centered about 0° where the coupling efficiency measures approximately 4%. For this phase angle, the coils are operating in phase. The highest efficiency is given by -75° . This outlier is likely due to the vacuum shot referenced for the coupling efficiency calculation being a different phase than the actual plasma loaded condition.

Although discharging the RMF coils in phase resulted in a higher coupling efficiency, we continued operating at a 90° phase angle to retain the RMF structure outlined by the theoretical model presented in Section III. Discharging the coils in phase with each other also increases the coupling efficiency per Fig. 20. This is likely due to a stronger peak electric field which assists the ionization process.

References

- [1] Jahn, R. G., *Physics of Electric Propulsion*, McGraw-Hill, New York, 1968.
- [2] Jankovsky, R., Tverdokhlebov, S., and Manzella, D., "High Power Hall Thrusters," *35th Joint Propulsion Conference*, 1999, pp. AIAA-99-315745.
- [3] Polzin, K. A., Martin, A. K., Eskridge, R. H., Kimberlin, A. C., Addona, B. M., Devineni, A. P., Dugal-Whitehead, N. R., and Hallock, A. K., "Summary of the 2012 Inductive Pulsed Plasma Thruster Development and Testing Program," Tech. Rep. NASA/TP-2013-217488, NASA-Marshall Space Flight Center, Huntsville, AL, 2013.
- [4] Polzin, K., Martin, A., Little, J., Promislow, C., Jorns, B., and Woods, J., "State-of-the-Art and Advancement Paths for Inductive Pulsed Plasma Thrusters," *Aerospace*, Vol. 7, No. 8, 2020, p. 105. <https://doi.org/10.1103/PhysRevLett.107.235001>.
- [5] Justin, K., Martin, R., and Sousa, E. M., "High Fidelity Modeling of Field-Reversed Configuration (FRC) Thrusters," Tech. Rep. AFRL-RQ-ED-TR-2017-0002, Air Force Research Laboratory, Edwards AFB, CA, 2017.
- [6] Weber, T., "The electrodeless Lorentz force thruster experiment," Ph.D. thesis, University of Washington, 2010.
- [7] Slough, J., Kirtley, D., and Weber, T., "Pulsed plasmoid propulsion: The ELF thruster," *31st International Electric Propulsion Conference*, 2009. IEPC paper 2009-265.
- [8] Slough, J., and Votroubek, G., "Magnetically accelerated plasmoid (MAP) propulsion," *42nd AIAA/ASME/SAE/ASEE Joint Propulsion Conference & Exhibit*, 2006. <https://doi.org/10.2514/6.2006-4654>, AIAA paper 2004-4654.
- [9] Blevin, H. A., and Thonemann, P. C., "Plasma confinement using an alternating magnetic field," *Conference on Plasma Physics and Controlled Nuclear Fusion Research, Nuclear Fusion Supplement, Part 1*, 1962, pp. 55-60.

- [10] Woods, J. M., Sercel, C. L., Gill, T. M., Viges, E., and Jorns, B. A., "Data-Driven Approach to Modeling and Development of a 30 kW Field-reversed Configuration Thruster," *36th International Electric Propulsion Conference*, 2019. IEPC paper 2019-717.
- [11] Weber, T. E., Slough, J. T., and Kirtley, D., "The electrodeless Lorentz force (ELF) thruster experimental facility," *Review of Scientific Instruments*, Vol. 83, No. 11, 2012, p. 113509. <https://doi.org/10.1063/1.4759000>.
- [12] Cusson, S. E., Hofer, R. R., Goebel, D. M., Georjgin, M. P., Vazsonyi, A. R., Jorns, B. A., and Gallimore, A. D., "A 30-kW Class Magnetically Shielded Nested Hall Thruster," *31st International Electric Propulsion Conference*, Vienna, Austria, 2019.
- [13] Wong, A. R., Toftul, A., Polzin, K. A., and Pearson, J. B., "Non-contact thrust stand calibration method for repetitively pulsed electric thrusters," *Review of Scientific Instruments*, Vol. 83, No. 2, 2012, p. 025103. <https://doi.org/10.1063/1.3680557>.
- [14] Viges, E. A., Jorns, B. A., Gallimore, A. D., and Sheehan, J. P., "University of Michigan's Upgraded Large Vacuum Test Facility," *36th International Electric Propulsion Conference*, 2019. IEPC-2019-653.
- [15] Jones, I. R., and Hugrass, W. N., "Steady-state solutions for the penetration of a rotating magnetic field into a plasma column," *Journal of Plasma Physics*, Vol. 26, 1981, pp. 441–453. <https://doi.org/10.1017/S0022377800010837>.